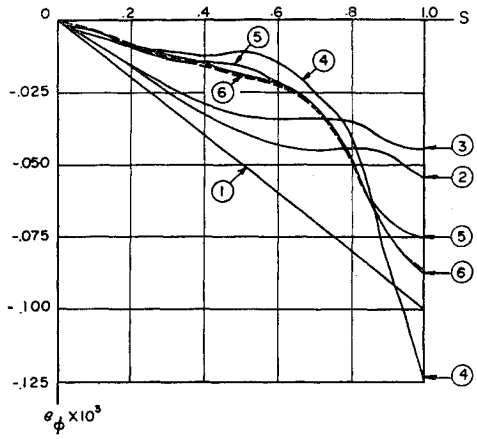

Fig. 2a The longitudinal strain used as the control variable in the stress analysis of a conical shell. The encircled numbers indicate the sequence of iterations performed. The dotted line indicates the solution based on the membrane theory and the homogeneous solution.

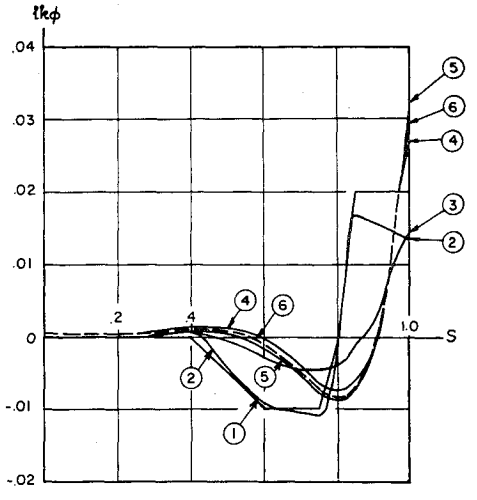

Fig. 2b The longitudinal curvature change used as the control variable in the stress analysis of a conical shell. The encircled numbers indicate the sequence of iterations performed. The dotted line indicates the solution based on the membrane theory and the homogeneous solution.

For the two control variables e_ϕ, k_ϕ, we assume the starting values throughout the range $s = (0,l)$ as shown by curves marked (1) in Fig. 2. The displacements u, w at $s = 0$ are assumed to be zero. We further adapt the following data in the computation: $l/h = 53.034$, $E = 30 \times 10^6$ psi, $p_z = 80$ psi, $h = \frac{1}{2}$ in., $\nu = \frac{1}{3}$, and $\beta = 60°$. The resulting control variable data during various steps of optimization are plotted in Fig. 2. Also plotted are the same data based on the membrane theory and the homogeneous solution. Based on the control variable data and the corresponding values of u, w, and ψ given by Eqs. (21–23), the stress data $N_\phi, N_\theta, M_\phi, M_\theta$ can be obtained from Eqs. (9–16).

Conclusion

In the optimum programming process, the control variables are selected in such a manner that the system can be defined completely with a set of first-order nonlinear differential equations. The control variables appear in both the derivatives of the state variables and the optimized function. In the shell stress problem, the strain variables are chosen as the control variables such that the deformation pattern of the shell is defined. An arbitrarily selected deformation pattern yields higher potential energy in the shell structure under the given load condition as compared to the actual case. Gradual optimization of the potential energy in the shell structure leads to the actual strain and deformation patterns. As the method is a numerical one, many nonlinear shell stress problems not subject to classical analysis can be handled in this manner.

During the optimization process, some judgment is needed in determining the square root mean (δP) of the amplitude change in control variables and the weighting functions W,Y. In general, (δP) should be reduced gradually when the optimization process approaches its final solution. The weighting functions should be arranged in such a way that the more sensitive areas have a higher weighting value.

In the numerical example, the obtained results based on optimum programming compare favorably with the available data based on the membrane and homogeneous solutions.

References

[1] Bliss, G. A., *Mathematics for Exterior Ballistics* (John Wiley & Sons Inc., New York, 1944), 1st ed., Chap. 5, pp. 63–97.

[2] Tsien, H. S., *Engineering Cybernetics* (McGraw-Hill Book Co. Inc., New York, 1954), 1st ed., Chap. 13, pp. 178–197.

[3] Bryson, A. E. and Denham, W. F., "A steepest-ascent method for solving optimum programming problems," J. Appl. Mech. **29**, 247 (1962).

[4] Timoshenko, S. and Woinowsky-Krieger, S., *Theory of Plates and Shells* (McGraw-Hill Book Co. Inc., New York, 1959), 2nd ed., Chap. 16, p. 533.

Mode Shape Effects on Winged Booster Stability

ROBERT L. SWAIM*
Air Force Flight Dynamics Laboratory, Wright-Patterson Air Force Base, Ohio

As future boosters become larger and more flexible, their elastic normal mode frequencies will decrease and narrow the margin between the first elastic mode frequency and the rigid body short-period frequency. When these frequencies become of the same order of magnitude, a coupling phenomenon which may result in an instability in either or both modes can occur. The coupling is particularly severe when the booster has a lifting payload and/or stabilizing fins.

The purpose of this note is to indicate the sensitivity of this coupling to small variations in elastic mode shape. If it is highly sensitive, then the elastic modes must be determined very accurately in order to ensure an accurate determination of the vehicle's forward-loop dynamic stability characteristics. There is somewhat of a paradox here in that the flexible modes become more difficult to determine, either analytically or experimentally, as the boosters become larger. This is due, in large part, to relative motion between structural elements.

When this coupling is very sensitive to mode shape variations, or what is analogous, errors in mode shape determination, the task of designing a suitable control system becomes extremely difficult. In order to maintain transient aerodynamic loading within prescribed limits, it is necessary to provide means of maintaining the desired degree of damping of transient rigid-body oscillations about a nominal trajectory. This must be done primarily by the control system. If small elastic mode shape variations cause wide excursions in short-period damping, the actuation devices would have to be capable of higher frequency response.

The design of a control system with minimum compensation demands an accurate knowledge of the elastic mode shapes and frequencies. As uncertainty in the knowledge of

Received February 1, 1963; revision received July 12, 1963. This work was sponsored in whole by the U.S. Air Force under Project 8219, Task 821901.

* Senior Research Engineer. Member AIAA.

the parameters to be controlled increases, the control system elements must be capable of successful operation over a wider range of parameter variations. This requires increased complexity and more sophisticated system components. In the case of strong modal coupling with resultant large changes in vehicle dynamics due to small errors in elastic mode shape knowledge, the control system performance required may be beyond the capabilities of existing hardware.

Two design philosophies are apparent: 1) concentrate on obtaining highly accurate input data for all flight conditions enabling design of the least complex control system; and 2) accept inaccuracies in data and concentrate on development of sophisticated control system components and combinations. In practice, a combination of the two approaches would most likely be used.

The point might be raised that adaptive systems have been developed to handle variations in the forward-loop dynamics. But keep in mind that these variations must be relatively small, i.e., small changes in frequency and damping. It will be pointed out later that when rigid-body and elastic-mode frequencies are in close proximity, the changes in forward-loop dynamics can be drastic for relatively small elastic mode shape variations.

In order to demonstrate this coupling phenomenon, a large, Saturn-type booster with a lifting payload was analyzed. The booster was provided with sufficient fin area to make it aerodynamically statically stable. Admittedly, a booster of this type is not likely to be statically stable; it would rely on the control system for stability. However, in this particular example we are interested in looking at the forward-loop coupling phenomenon in the absence of the control system. This requires a statically stable vehicle. The coupling is less severe but can still be serious as fin area is reduced and its function taken over by the control system.

The essence of the coupling can be shown by considering only three degrees of freedom, rigid pitch and plunge, and the first elastic-body bending mode. Quasi-steady aerodynamics acting on the payload and fins are assumed, with aerodynamic forces on the booster body being assumed negligible for simplicity. The dynamic pressure is 1000 psf. With reference to stability axes, the equations of motion can be put in the following matrix form involving the Laplace transformation:

$$\left[\begin{array}{c|c|c} (b_{11}s + c_{11}) & (c_{12}) & (b_{13}s + c_{13}) \\ (c_{21}) & (b_{22}s + c_{22}) & (b_{23}s + c_{23}) \\ \hline (c_{31}) & (c_{32}) & (a_{33}s^2 + b_{33}s + c_{33}) \end{array}\right] \times \left\{\begin{array}{c} \alpha(s) \\ \dot{\theta}(s) \\ q(s) \end{array}\right\} = 0 \quad (1)$$

α is angle of attack, $\dot{\theta}$ is pitch rate, and q is the elastic mode generalized coordinate. a_{ij}, b_{ij}, and c_{ij} are constant coefficients for the time instant considered. The terms coupling the elastic mode and rigid-body equations are located in the upper-right and lower-left quadrants of the partitioned square matrix. The determinant of the matrix can be expanded to give the following characteristic equation:

$$(a_{33}s^2 + b_{33}s + c_{33}) \begin{vmatrix} (b_{11}s + c_{11}) & (c_{12}) \\ (c_{21}) & (b_{22}s + c_{22}) \end{vmatrix} - c_{32} \begin{vmatrix} (b_{11}s + c_{11}) & (b_{13}s + c_{13}) \\ (c_{21}) & (b_{23}s + c_{23}) \end{vmatrix} + c_{31} \begin{vmatrix} (c_{12}) & (b_{13}s + c_{13}) \\ (b_{22}s + c_{22}) & (b_{23}s + c_{23}) \end{vmatrix} = 0 \quad (2)$$

All the terms contributing to the coupling are contained in the last two of the three determinant products. The only elastic parameters occurring in these terms are mode deflections and slopes; the undamped elastic mode natural frequency and structural damping ratio appear only in the first determinant product.

Expansion of the first determinant in Eq. (2) yields an "uncoupled" rigid-body short-period frequency of 1.17 rad/sec and a damping ratio of 0.074. Using a typical assumed elastic mode with a natural frequency of 3.14 rad/sec and structural damping of 0.01 (case 1 of Fig. 1) and solving for the roots of Eq. (2), yields a "coupled" short-period frequency of 1.35 rad/sec and damping ratio of 0.153. The "coupled" elastic-mode frequency and damping ratio are 2.48 rad/sec and -0.016, respectively. We see that for this assumed mode shape the elastic mode is unstable.

Now, varying only the mode shape slightly (case 2 of Fig. 1) with the same undamped natural frequency and again solving Eq. (2), one gets a stable "coupled" elastic mode with a frequency of 2.65 rad/sec and damping ratio of 0.021. However, the significant result is that the short-period mode contains a positive and negative real root, 0.534 and -0.278. This indicates the coupling phenomenon has produced a rigid-body static divergence, even though the vehicle is aerodynamically statically stable.

To point up the fact that the coupling is highly dependent on frequency proximity, cases 1 and 2 were analyzed again with the only change being that the elastic mode natural frequency was raised a factor of 10 to 31.4 rad/sec with no change in mode shapes. The short-period frequency and damping ratio were 1.16 rad/sec and 0.073, respectively, for both cases. These are nearly identical with the "uncoupled" values of 1.17 rad/sec and 0.074. The "coupled" elastic mode frequency and damping ratios for both cases were 31.3 rad/sec and 0.012.

It is evident from the forementioned results that the coupling is highly sensitive to elastic mode shape when rigid-body and elastic mode frequencies are of the same order of magnitude. It was also determined through algebraic and numerical analysis of Eq. (2) that the principal parameter controlling the strength or severity of the coupling is the sum of the products of the normal force curve slope and normalized elastic mode deflections at the centers of pressure of the lifting payload and stabilizing fins. Complete details of this analysis may be found in Ref. 1.

Additional work has been done, with equally interesting results, on determining the effects on the coupling phenomenon of removing the fins and adding a feedback control and stabilization system.[2, 3]

Historically, unstable coupling between two or more elastic modes has been termed "flutter." This is the domain of the aeroelastician. The stability and control analyst has been concerned with the low frequency interaction of rigid-body and elastic modes. The higher frequency flutter phenomena have seldom effected his analysis. The flight control analyst has patterned his work about the stability and control man's methods, since the flutter problems of the aeroelastician have

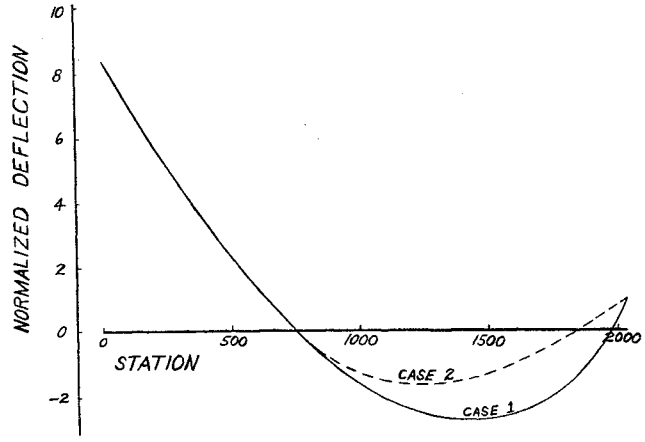

Fig. 1 Elastic mode shapes.

not, in general, entered into his control problems. This classical separation of the three fields of analysis has led to a general lack of understanding, coordination, and communication between aeroelasticians and flight control analysts. This is, indeed, unfortunate. These people are all working on the same problem area and, if you will, the same equations of motion—the major difference being the frequency range of interest. Aeroelasticians are interested primarily in the higher frequencies and flight control analysts in low frequency and rigid-body dynamics. It is also unfortunate that separate departments have been set up by most companies to deal with the two areas; this has served to widen the technical communication gap.

In the very near future, as advanced vehicles become more flexible, the flutter-type dynamics are going to present problems in the design of the flight control system. The increased structural flexibility will require control system bandwidths of operation to be increased while the elastic mode frequencies are tending downward, with the result that the pure flutter dynamics may feed energy into the control system dynamics as well as the vehicle rigid-body modes. This could result in an extremely complex three-way coupling problem. To effectively cope with this type of situation, it is imperative that aeroelasticians, stability and control analysts, and flight control analysts mount their attack of the problem on a more common analysis ground than exists between the three groups today. An important first step in this direction would be for companies and agencies to merge these people into truly unified dynamic analysis departments.

References

[1] Swaim, R. L., "Effect of low-frequency elastic mode shape on forward-loop stability characteristics of winged boosters," Air Force Flight Dynamics Lab. ASRMCM-TM-62-8 (July 1962).

[2] Swaim, R. L., "Closed-loop stability of a winged-payload booster subject to variations of an elastic mode shape," Air Force Flight Dynamics Lab. ASRMCM-TM-62-11 (November 1962).

[3] Swaim, R. L., "Further investigation of elastic mode effects on closed-loop stability of a winged booster," Air Force Flight Dynamics Lab. ASRMCM-TM-63-1 (April 1963).

Planar-Wound Filamentary Pressure Vessels

R. F. HARTUNG*
Lockheed Missiles and Space Company, Palo Alto, Calif.

FIGURE 1 depicts a dome with base radius R suitable for the end closure of a pressure vessel and formed by winding resin-coated high-strength filaments onto a mandrel and then heat-treating the resulting structure to produce a hard and resistant composite. The filaments are deposited along lines defined by the intersection of the surface with a plane making an angle γ with the axis of revolution z. Such a winding pattern leads to what will be referred to as a planar-wound filamentary structure. It is further assumed that the filaments are always deposited in pairs that are symmetric with respect to a meridian.

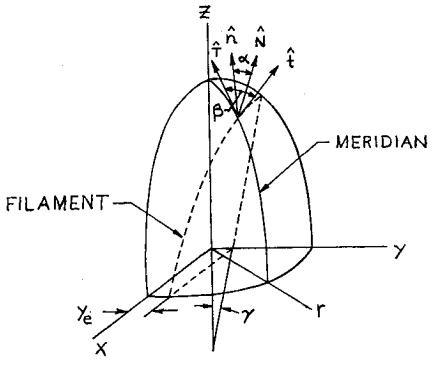

Fig. 1 Typical planar-wound dome and associated geometry.

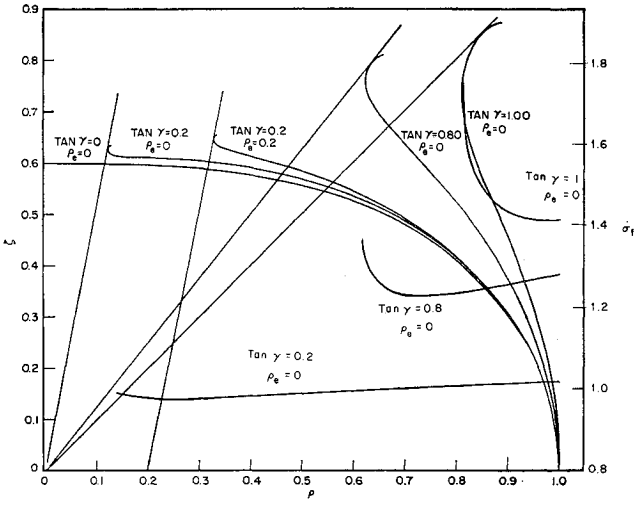

Fig. 2 Balanced design planar-wound dome contours and associated stresses.

If the dome meridian curve is defined by

$$r = r(z) \tag{1}$$

then the principal radii of curvature in the meridional and circumferential directions, respectively, are

$$r_1 = -(1 + r'^2)^{3/2}/r'' \qquad r_2 = r(1 + r'^2)^{1/2} \tag{2}$$

where primes denote differentiation with respect to z. For a closed dome in equilibrium under the action of uniform pressure p and in the absence of axial load, the meridional and circumferential stress resultants are, respectively,†

$$N_\phi = pr_2/2 \qquad N_\phi = (pr_2/2)[2 - (r_2/r_1)] \tag{3}$$

Projection of the filament curve on the (y,z) plane gives

$$x^2 = r^2 - (y_e + z\tan\gamma)^2 \tag{4}$$

y_e is defined in Fig. 1. An expression for the winding angle β between the meridian curve and filament curve is obtained from the definition

$$\cos\beta = \hat{t}\cdot\hat{T} \tag{5}$$

$\hat{T}$ and $\hat{t}$ being the unit tangent vectors of the meridian and filament curves, respectively. Combining (4) and (5), one obtains

$$\tan^2\beta = \frac{[\rho\dot{\rho} - (\rho_e + \zeta\tan\gamma)\tan\gamma]^2 + (\tan^2\gamma - \dot{\rho}^2)[\rho^2 - (\rho_e + \zeta\tan\gamma)^2]}{(1 + \dot{\rho}^2)[\rho^2 - (\rho_e + \zeta\tan\gamma)^2]} \tag{6}$$

where

$$\rho = \frac{r}{R} \qquad \zeta = \frac{z}{R} \qquad \rho_e = \frac{y_e}{R} \qquad (\dot{}) = \frac{d(\ )}{d\zeta}$$

Presented at the AIAA Launch and Space Vehicle Shell Structures Conference, Palm Springs, Calif., April 1–3, 1963; revision received September 12, 1963.

* Member, Mechanical and Mathematical Sciences Laboratory.

† Limitations on the use of (3) for orthotropic shells are discussed in Ref. 1.